Dalton Transactions

Accepted Manuscript

ROYAL SOCIETY OF CHEMISTRY

www.rsc.org/dalton

Article Title

Synthesis, Characterization and Biocompatibility of Chitosan functionalized superparamagnetic nanoparticles for heat activated curing of cancer cells

Running Title

Chitosan –LSMO and hyperthermia

Authors

N. D. Thorat[a], S. V. Otari[b], R. M. Patil[b], R. A. Bohara[b], H. M. Yadav[b], V. B. Koli[b], A. K. Chaurasia[ac]* and R S. Ningthoujam[d]

[a]Samsung Biomedical Research Institute, School of Medicine, Department of Molecular Cell Biology, Sungkyunkwan University, Suwon 440-746, South Korea

[b]Center for Interdisciplinary Research, D. Y. Patil University, Kolhapur 416006, India

[c] Molecular Biology Division, Bhabha Atomic Research Centre, Mumbai 400085, India

[d] Chemistry Division, Bhabha Atomic Research Centre, Mumbai 400085, India

***CORRESPONDING AUTHOR**

School of Medicine,
Samsung Biomedical Research Institute
Laboratory of Structural Biology
Department of Molecular Cell Biology
Sunkyunkwan University, South Korea-440746
Phone: +82-31-299-6150
Fax: +82-31-299-6159
E-mail: chaurasia@skku.edu, chaurasia.ak@gmail.com

Abstract:

Surface functionalization, colloidal stability and biocompatibility of magnetic nanoparticles are crucial for their biological applications. Here, we report a synthetic approach for direct preparation of a superparamagnetic nanoparticles consisting of perovskite LSMO core modified with covalently linked chitosan shell that provides colloidal stability in aqueous solutions for cancer hyperthermia therapy. The characterization of core-shell nanostructures using Fourier transform infrared spectroscopy, thermo-gravimetric analysis to assess the chemical bonding of chitosan to nanoparticles; field-emission scanning electron microscopy and transmission electron microscopy for its size and coating efficiency estimation and magnetic measurement system for their magnetization properties were performed. Zeta potential and light scattering studies of core shell displayed to possess good colloidal stability. The confocal microscopy and MTT assay is performed for qualitative and quantitative measurement of cell viability and biocompatibility. In depth cell morphology and biocompatibility is evaluated by using with multiple-staining of different dyes. The magnetic@chitosan nanostructure system is found to be biocompatible up to 48 h with 80% cell viability. Finally, *in vitro* cancer hyperthermia study is done on MCF7 cell line. During *in vitro* hyperthermia cancer, cell viability is reduced upto 40% within 120 min for chitosan coated nanoparticles. Our results demonstrate that this simplified and facile synthesis strategy show potential for designing colloidal state stable and biocompatible core shell nanostructures for cancer hyperthermia therapy.

1. Introduction

The surface functional groups on the nanoparticles (NPs)plays significant role in the biological applications and need to be appropriately conjugated with biological moiety. In the absence of an efficient surface coating, the agglomeration and aggregation of magnetic nanoparticles mainly through van der Waals attraction destabilizes the suspension of magnetic nanoparticles in aqueous suspension. Biochemically surface functionalized magnetic nanoparticles can be used in a wide variety of biological applications, such as magnetic resonance imaging (MRI), hyperthermia, targeted drug delivery, cell imaging and capture and detection pathogenic bacteria etc.[1-4] For the successful application of these NPs in biomedical field, the surface of is typically modified with polymer molecules to ensure the parameters such as **a**) their colloidal stability; **b**) biocompatibility; **c**) effective bio-distribution; and **d**) prevention of their rapid clearance by the reticular endothelial system[5]. The most significant application of magnetic nanoparticles is the cancer hyperthermia therapy, in which cancerous cells or tumors can be cured or destroyed by elevating its temperature in the range of 42-46 $^{\circ}$C by using MNPs and application of an external alternating magnetic field[6, 7].

For the efficient coating of magnetic nanoparticles to maintain their colloidal properties and biocompatibility, a variety of surfactants from polymeric to non-polymeric molecules such as lipids and proteins are used to coat magnetic nanoparticles to prevent aggregation caused by magnetic dipole–dipole attractions between nanoparticles[1]. Among a wide spectrum of coating materials, chitosan may be considered as one of the important candidates because of its excellent biocompatibility, low toxicity and commendable biodegradability. Biological activities such as antimicrobial activity and low immunogenicity would prove chitosan, as an attractive candidate for nanobiotechnological applications[8].

The prominent application of magnetic nanoparticles is in magnetic fluid hyperthermia therapy. The study is focused on the construction of magnetic/chitosan (core/shell) nanocomposites for magnetic fluid hyperthermia application. The core magnetic material used for the study is $La_{0.7}Sr_{0.3}MnO_3$ (LSMO). LSMO is a multifunctional compound and has shown many applications in MRI, drug delivery and hyperthermia in recent years[9-12]. However, LSMO biocompatibility, colloidal stability and particle bio-distribution, high Curie temperature and low saturation magnetization remained pertinent problems at variable degree for various nanocomposites. The low Curie temperature and high saturation magnetization is a favorable criterion for hyperthermia application and LSMO particularly $La_{0.7}Sr_{0.3}MnO_3$compound satisfies the condition hence, it is studied for hyperthermia therapy.

In this study, we describe a reproducible technique for the preparation of magnetic core/shell superparamagnetic NPs consisting of a LSMO nucleus ($La_{0.7}Sr_{0.3}MnO_3$) and a chitosan shell. The coating efficiency of chitosan around the magnetic core has been analyzed using Fourier transform infrared spectrometry (FTIR), thermogravimetric analysis (TGA), electron microscopy (FSEM and TEM). The magnetic properties of these core/shell structures were evaluated in order to analyze MNPs' magnetic responsiveness by using Vibrating Sample Magnetometer (VSM). The heat production (hyperthermia effect) of the LSMO/chitosan core/shell nanocomposites under the influence of an oscillating magnetic gradient was also examined. The biocompatibility is evaluated by using MTT assay. Further, the in-depth cell-nanoparticle interaction was studied by confocal laser scanning microscopy (CLSM) with multiple staining of fluorescein isothiocyanate (FITC), propidium iodide (PI) and 4',6-diamidino-2-phenylindole (DAPI). Finally, the effect of hyperthermia produced by these core/shell

nanostructures is evaluated on normal and cancer cells *in vitro* and found to be a vital biological application in cancer therapy.

2. Experimental

2.1 Synthesis of LSMO@Chitosan nanostructures

The perovskite type $La_{0.7}Sr_{0.3}MnO_3$ (MNPs) have been prepared by the method described earlier[13]. Chitosan functionalized LSMO superparamagnetic nanocomposites (CH-MNPs) with a core–shell structure were prepared by suspension cross-linking method. This procedure was carried out in a 100-ml round-bottomed four-necked flask equipped with a mechanical stirrer, an inlet of nitrogen and a condenser. LSMO (0.2 g) were dispersed in a solution with 10ml paraffin and 1ml span-80 and then 30 mL solution of chitosan in acetic acid with concentration of 2% was added. pH of the whole system is maintained neutral (pH 7.0) so that MNPs can easily disperse in solution during experiment. The molar ratio of chitosan and LSMO was 1:1. The suspension was mixed by ultrasonic irradiation for 60 min. Then the core shell formation was allowed to proceed for 5 h at 50 $^{\circ}$C under mechanical stirring (1000 rpm). The product were dialyzed and purified by magnetic field separation and decantation with water and ethanol. This washing procedure was repeated five times. The final chitosan capped MNPs were dried in a vacuum atmosphere at 60 $^{\circ}$C for 10 h.

2.2. Characterization

2.2.1. Physical characterizations

Thermal decomposition behavior of the CH-MNPs precursors was studied on a Du Pont 2100 thermal analyzer on 6–7 mg samples in nitrogen with a scanning rate of 10 $^{\circ}$C min^{-1}. The Fourier

Transform Infrared spectroscopy (FTIR) measurements were carried out on a Perkin-Elmer spectrometer (Model No.783, USA) in the range 400 to 4000 cm^{-1}. More distinct surface morphology and particle size have been observed by Field Emission-Scanning Electron Microscopes (FESEM-Model JSM-7600F). The particle size and shape was determined by Transmission Electron Microscopy (TEM, Philips CM200 model, operating voltage 20-200kV, resolution 2.4 Å).The magnetization quantification was performed on a Quantum Design SQUID magnetometer.

Zeta potential measurements were performed by using a PSS-NICOMP- 380 ZLS (USA) particle sizing system. Measurements were taken in water HCl and NaOH are used to tune the pH of water from 2 to 12. The reported zeta potential values are an average of three measurements, each of which was obtained over 30 electrode cycles. Induction heating of LSMO MNPs for hyperthermia application was performed in plastic micro centrifuge tube (1.5 mL) by using an induction heating unit (Easy Heat 8310, Ambrell; UK) with 6 cm diameter (4 turns) heating coil. A provision of water circulation in the coil was made to keep the temperature of the coil at ambient temperature. MNPs and CH-MNPs are suspended in 1 mL of distilled water placed at the center of the coil and the applied frequency was 265 kHz. Particles were dispersed in water with concentration 10 mg/mL and ultrasonicated for 20 min for getting well dispersion of the MNPs in aqueous solutions. Samples were heated for 10 min with the desired current (200 to 600 A, 83.8 to 502.8 Oe). Temperature was measured using optical fiber probe with an accuracy 0.1 $^{\circ}C$.

2.2.2. Biocompatibility study

2.2.2.1. Cell culture

The comparative *in vitro* cytotoxicity study of MNPs and CH-MNPs was done on L929 HeLa and MCF7 cells obtained from National Centre for Cell Sciences, Pune (India) and detailed toxicity study was done in the National Toxicology Centre Pune (ISO 10993/USP 32 NF 27). The L929 cells were grown in DMEM (Dulbecco's Modified Eagle Medium) supplemented with 10% v/v fetal bovine serum, kanamycin (0.1 mg/mL), penicillin G (100 U/mL), and sodium bicarbonate (1.5 mg/mL) at 37 $^{\circ}$C in a 5% CO_2 atmosphere. HeLa and MCF7 cells were grown in MEM + 10% FBS + Antibiotics at 37 $^{\circ}$C in a 5% CO_2 atmosphere.

2.2.2.2. MTT Assay

L929, HeLa and MCF7 cells were incubated with the concentration of 2×10^5 cells/mL in respective medium for 24 h in a 96- well microtire plate. After 24 h, the old media was replaced by fresh media and different proportions of sterile MNPs and CH-MNPs (0.2, 0.4, 0.6, 0.8 and 1 mg/mL of culture media). The plates containing cells with variable amount of MNPs CH-MNPs were incubated at 37 $^{\circ}$C in a 5% CO_2 atmosphere for 24 and 48 h. After 24 and 48 h, the 10 µL MTT solution was added into each well including control wells. The plates were incubated for 3 h at 37 $^{\circ}$C in a 5% CO_2 atmosphere for metabolism of MTT with the NPs and cell media. Then the total medium was removed by flicking the plates and only anchored cells remained in the wells. The cells were then washed with PBS and formed formazon was extracted in 200 µL acidic Isopropanol. Finally, absorbance was read at 570 nm and from that the cell viability was calculated. The experiments were replicated three times and the data were graphically presented as mean ± SD. The relative cell viability (%) compared with control cells without nanoparticles are calculated by the equation: $[A_{absorbance}]_{tested} / [A_{absorbance}]_{control} \times 100$.

2.2.2.3. Confocal microscopy study

L929 cells (2×10^5 cells/mL) were grown into DMEM and were transferred to the slide petri dishes in 2 mL DMEM. The cells were kept in slide petri dishes for more 24 h for growing, the cell culture media was changed to new DMEM media and varying (0, 0.2, 0.4, 0.6, 0.8 and 1 mg/mL) concentration of nanoparticle were added. L929 cells with or without nanoparticle were incubated in CO_2 incubator for 24 h. The media were removed and washed 3 times with PBS (pH 7.4). After washing, the cells were stained with Fluorescein isothiocyanate (FITC), propidium iodide (PI) and 4',6-diamidino-2-phenylindole(DAPI) (1 ug/mL) for 5 min. Then the stained cells were washed with PBS for 3 times. Finally, cells were overlay with 400 micro liters PBS and directly observed (without cell fixation) under confocal microscope (at 40X magnifications Zeiss LSM 510 Meta). Red, blue and green fluorescent cells were observed by excitation and emission PI ($\lambda_{excitation\ =}$ 535 nm, $\lambda_{emission}$ 617 nm), DAPI ($\lambda_{excitation}$ 358 nm, $\lambda_{emission\ ,}$ 461 nm) and FITC ($\lambda_{excitation}$ 495 nm, $\lambda_{emission}$ 519 nm) and detected with a band-pass filter and the final images were generated by superimposing red, blue and green images.

3. Results and Discussions

3.1 FTIR, TGA, FESEM and TEM analysis of LSMO functionalization with Chitosan

The uniform coating of chitosan polymer on MNPs surface is evaluated by FTIR, TGA, FESEM and TEM study. The chitosan coating experimental step is optimized well to get uniform layer of chitosan on MNPs surface. In the present study, FTIR tool is applied to find out the chitosan functional groups on MNPs surface, the obtained spectrum for chitosan modified MNPs is shown in fig.1. The FTIR spectrum of bare MNPs is already published in our earlier study[13].The bands observed at 600 cm^{-1} is assigned to the Mn-O bonding from the LSMO (Fig. 1a). The characteristic peak observed at 1000 cm^{-1} is ascribes to C–O stretching of primary alcoholic

group in chitosan. The peaks observed at 1403 cm^{-1}, 2854 and 2924 cm^{-1}represent to C–H stretching. The peak observed at 1627 cm^{-1} is a characteristic peak of N–H bending vibration and represents efficient coating of chitosan on LSMO MNPs (Fig. 1a).The broad band observed at around 3400 corresponds to stretching vibration of O–H. The FTIR results are well comparable with the earlier reports on chitosan capped magnetic nanoparticles[14-17].

Fig.1b shows thermogravimetric (TG) curves of MNPs and CH-MNPs measured by a thermogravimetric analyzer. As TG was performed under N_2 atmosphere, the oxidation of NPs was greatly reduced. The Thermogravimetric analysis provides additional quantitative evidence on the structure of coating on surface of nanoparticles. 3% weight loss due to evaporation of physically adsorbed water in the temperature range below 110 $^{\circ}C$ was observed for CH-MNPs sample. Two major weight loss stages are observed in thermogram for CH-MNPs, one below 110 $^{\circ}C$ (a region) which can be ascribed to evaporation of water, while the other one beginning at about 140 $^{\circ}C$ (b region) due to the decomposition of chitosan molecules. The differences in total weight loss for both samples help us to calculate the percentage chitosan molecules attached to the surface of nanoparticles. Thus, it is assumed that about 13% of chitosan polymeric molecules are adsorbed on to the surface of nanoparticles. Above the temperature of 350 $^{\circ}C$ (region c) both samples attain stability in terms of weight loss. Fig. 1(c) and (d) shows the FESEM and TEM images of CH-MNPs. The particles are almost spherical with diameters ranging from 20 to 30 nm. Most of the particles are mono disperse while some agglomerated due to magneto-dipole interactions between particles.

3.2 Magnetization behavior of MNPs and CH-MNPs

The magnetization behavior of MNPs and CH-MNPs is carried out in order to understand the effect of coating on magnetic properties. The M *vs* H measurements as a function of applied field

are shown in fig. 2. On the basis of SQUID-VSM measurements, it can be seen from the hysteresis curves for bare and functionalized MNPs 300 K that almost negligible coercivity or remanence existed, indicating the superparamagnetic behavior of MNPs before and after coating. The values of magnetization for MNPs and CH-MNPs are 44 and 40 emu/g, respectively. The magnetization decreased with coating of chitosan, this is because magnetization is proportional to the amount of weight for the same magnetic material. Organic coating layers (chitosan) on magnetic material increase the amount of non-magnetic substance which reduces the overall magnetization of the material.

3.3 Colloidal stability of CH-MNPs core shell nanostructure

The effect of pH on colloidal stability of chitosan capped MNPs is evaluated by using zeta potential technique and the obtained data is presented in the fig. 3. The zeta potentials of CH-MNPs are 31.56, 18, 9.11,1 and -11.38 mV at pH 2,4,6,8 and 10, respectively. The zeta potential of coated particles is positive in the range of pH 2.0–7.0, this indicates the presence of positive charges on the CH-MNPs surface. The increase in positive zeta potential with a decrease in pH,is attributed to the protonation of free amino groups at low pH. These protonated amino groups provide enough charge to stabilize coated nanoparticles in acidic pH. The isoelectric point (IEP) of chitosan is around 6.3 hence, the chitosan capped particles are colloidal less stable around this pH. In the present study, the IEP is shifted towards higher pH (~ 8) and it is because of combining effect of MNPs and chitosan[18, 19].

3.4 Biocompatibility of MNPs and CH-MNPs core shell nanostructures

To verify whether chitosan capped MNPs affected cellular activity, the prepared MNPs and CH-MNPs are incubated with HeLa and L929 and MCF7 cells. The MTT assay evaluates the mitochondria activity and therefore can be used as a method to test cell growth as well as cell

death[20]. The L929 and HeLa and MCF7 cell lines incubated with MNPs and CH-MNPs for 24 and 48 h, respectively, with the concentration of 0.2, 0.4, 0.6, 0.8, and 1 mg/mL at 37 °C in the 5% CO_2 atmosphere. Cell viability was measured using the MTT assay. From the cytotoxicity data, it is found that the cell viability gradually decreases with increasing both NPs concentration and incubation time. The corresponding data show negligible cellular toxicity for CH-MNPs (Fig. 4). A minute change is observed on the cell viability by different cell lines. The change is attributed to the different physical nature of the cells. The differences in cell viability data are most likely evoked by cellular characteristics, as each cell type has an individual surface property and cellular morphology even if each cell type shows a distinct metabolic activity. These parameters strongly influence CH-MNPs -cell interactions and viability [21]. However, results obtained are almost the same and no extreme change is observed. The cell viability of MNPs at 1 mg/mL concentration is about 80 and 75 % on L929 cells, 79 and 74% on HeLa cells and 80 and 79% on MCF7 cells for 24 and 48 h, respectively. The cell viability is increased after chitosan coating and for CH-MNPs it is about 86 and 81% on L929 cells, 85 and 81% on HeLa cells and 86 and 83% on MCF7 cells for 24 and 48 h, respectively.

3.5 Physical interaction of CH-MNPs and cellular phenotype study

To assure the validity of the MTT assay used to determine cell death and to identify the apoptosis and necrosis by CH-MNPs, we applied additional experiments using a confocal microscopy technique. The L929 cells are stained with DAPI, FITC and PI dyes for evaluating the cell toxicity by CH-MNPs. This type of multiple staining couple with microscopy observations identify dead and live cells more accurately and qualitatively[22]. Cell death mechanism was classified into two categories mainly apoptosis and necrosis. Necrosis is the

pathological process which occurs when cells are exposed to fast-acting metabolic poison or extreme variance in physiological conditions. Apoptosis, in contrast, is a programmed cell death that arises under normal physiological conditions[23]. Since FITC enters in to live cells and emit green (fluorescein) generated by the enzymatic hydrolysis of calcein-AM that only occurs in live cells and DAPI generally binds to nucleus of live cells and its fluorescence is strongly enhanced after binding while PI could only stain cells that had lost membrane integrity. Thus, live cells will be uniformly stained green, early apoptotic cells will be densely stained as green yellow or displayed green yellow fragments, while late apoptotic cells will be densely stained as orange or displayed orange fragments, and necrotic cells will be stained with orange with no condensed chromatin under the multiple staining[24]. The simultaneous staining of nucleus with DAPI and PI is advantageous and represents the accurate nature of live and dead cells[31]. After 24 h of MNPs treatment and compared with untreated cells (Fig. 5 a-f), characteristic of cell death, including cell shrinkage, few cellular extensions, increased floating cells were not observed in L929 cells exposed to CH-MNPs. However, very minute concentration dependent increase in the percentage of cells stained positive for PI was observed, indicating a loss of membrane integrity at higher concentrations.

Overall percentage of apoptotic and necrotic cells are statistically insignificant in CH-MNPs treated L929 cells with concentration 1 mg/mL for 24 h. Finally, we conclude that the apoptosis and necrosis of L929 cell lines by CH-MNPs is almost negligible. In addition, our results demonstrated that CH-MNPs reduced the viability of MCF7, HeLa and L929 cells in a concentration and time-dependent manner. Both the direct observation by using confocal microscope and MTT assay showed the CH-MNPs were no toxic and just only slightly toxic at high concentration.

From last couple of years our group has working on finding definite solution of LSMO material towards its safe biomedical applications. We developed LSMO nanoparticles by cost effective combustion synthesis and studied its biocompatibility. The uncoated LSMO nanoparticles synthesized by polyvinyl alcohol route shows 72% cell viability up to 48 h on HeLa cells for concentration of 1 mg/mL. Further, the cell viability of this material is improved by polymeric (dextran) coating and it is about 90 % and for nonpolymeric (betaine HCl) it is about 81%[29, 13]. We also examined the effect of LSMO-oleic acid and Pluronic F127 core shell formation on cell viability, and we found the cell viability is improved upto 89%[26]. In the present case cell viability is about 81% on same cell line with same concentration and time of incubation. The cell viability is low as compared to other polymers like Dextran and Pluronic F127, however, SAR values of this nanocomposite are improved compared to all others studied above and this is an additional advantage. Studies on improved SAR values and its effect on *in vitro* hyperthermia on cancer cells are presented in next section.

3.6 CH-MNPs in curing cancer cell by magnetic field mediated elevation of temperature

Fig. 6(a) represents the temperature kinetic curves obtained after application of an alternating magnetic field on both samples which were dispersed in water with a concentration of 2 mg/mL and (b) represents SAR vs. applied magnetic field of the same sample. Temperature kinetic curves show a rise in temperature is dependent on the applied magnetic field. Fig. 6(b) represents the specific absorption rate (SAR) values of chitosan coated LSMO MNPs in water. SAR values are also increased with increasing field strength. The heat generation by LSMO MNPs is governed by eddy current loss, hysteresis loss and relaxation loss. The in depth physical mechanism and mathematical expressions of these mechanisms are reviewed in recent literature[25-28]. The gradual increase in SAR is observed with increasing field (Fig. 6). The

observed SAR at applied magnetic field of 300 Oe is ~80 W/g. The SAR value for bare LSMO MNPs is ~45 W/g at applied field of 300 Oe. The significant increase in SAR is observed after coating with chitosan of LSMOMNP surface. The improved SAR is attributed to the well colloidal stability of functionalized LSMO MNPs over non-functionalized.

The efficacy of MNPs and CH-MNPs in the killing of human breast cancer cells (*in vitro* hyperthermia) was determined by a trypan blue viability assay and obtained results are shown in fig. 6 (c). During the experiment the temperature of the MNPs and CH-MNPs Cell solution is maintained in between 44-45 $^{\circ}$C. Temperature profile of the *in vitro* hyperthermia experiment on MCF7 cells for NPS and CH-MNPs is shown in fig. 6 (d). The exposure of the cells to the magnetic field in the absence of MNPs did not show any significant cytotoxic effect on cell viability, suggesting the alternating magnetic field used in current study is not harmful to human being. Compared to the untreated control, normal and cancer cells treated with MNPs showed 7 and 40% decrease in viability for 120 min of irradiation, respectively. The decrease in normal cell viability is due to the cell nanoparticle interactions and high elevated temperature. However, cancer cells treated with MNPs showed a 40% decrease in viability with respect to an untreated control. The normal and cancer cells without MNPs and treated with the field do not shows decrease in cell viability, suggesting the alternating magnetic field used in current study is not harmful to human being. However, the decrease in cancer cell viability after irradiation of alternating magnetic field clearly indicates the hyperthermia effect on cancer cells. Interestingly, we observed cancers killing by CH-MNPs are more predominant than bare MNPs, and this is attributed to the good colloidal stability of CH-MNPs in cell solution, which can efficiently generate and distribute heat to cancer cells within short time.

Magnetic fluid hyperthermia is an artificially induced heat treatment of a disease especially designed for cancer, uses temperatures ranging between 42-47 °C. Generally, a temperature below 45 °C induces apoptotic cell death. Because cancer cells are susceptible to heat at about 43 °C, while most normal cells remain undamaged[30]. In our present study, we shown killing rate of cancer cell over normal cell is higher and it supports the above conclusion. To find out the mechanism of cancer cell death by CH-MNPs we performed DAPI, FITC and PI staining correlated with confocal microscopy. Before AC magnetic field application, neither FITC nor PI-stained cells are detected (Fig. 6 e). After 1 h post-hyperthermia treatment, both FITC and PI-stained cells are observed, and this is because of membrane destruction by magnetic fluid hyperthermia. The membrane integrity loss by cancer cells indicates early-stage apoptosis (Fig. 6 e). Characteristic of cell death by apoptosis, including cell shrinkage, lost membrane integrity, few cellular extensions, increased floating cells are observed for cells treated with MFH. These results are thus fully consistent with the notion that CH-MNP hyperthermia occurs predominantly through apoptosis.

4. Conclusion

The present investigation reports synthesis of highly water dispersed superparamagnetic with chitosan core shell nanoparticles and its development towards for high performance magnetic fluid hyperthermia. The core shell formulation has improved colloidal stability, biocompatibility and hyperthermia properties efficiently. The core shell formulation improves cell viability and do not induces apoptosis and necrosis. The anticancer drug and fluorescent molecules loading is easily possible to this system and can be efficiently used for drug delivery and cancer hyperthermia in future. CH-MNPs magnetic nanocomposite has been anticipated an

additional advantage of being bactericidal. In bacterial cell (e.g. *Helicobacter pylori*) induced cancer, CH-MNPs can be used for both bacterial cell eradication by **a**) its bactericidal activity **b**) bacterial capture and cleaning by MNPs using external magnetic field and cancer cells curing by rapid temperature rise.

Author Contributions: The manuscript was written through contributions of all authors. All authors have given approval to the final version of the manuscript.

References

1. G. Unsoy, S. Yalcin, R. Khodadust, G. Gunduz and U. Gunduz, *J Nanopart Res*, 2012, **14**, 964.
2. D. Baba, Y. Seiko, T. Nakanishi, H. Zhang, A. Arakaki, T. Matsunaga and T. Osaka, *Colloids Surf B Biointerfaces*, 2012, **95**, 254.
3. R. A. Petros and J. M. DeSimone, *Nat Rev Drug Discov*, 2010, **9**, 615.
4. S. S.Nan, W. Chao, Z. Z. Zan, H. Y. Long, S. S Venkatraman, and S. S.Nan, *Chin. Phys. B*, 2014, **23**, 37503.
5. R. A. Frimpong and J. Z. Hilt, *Nanomedicine*, 2010, **5**, 1401.
6. V. Singh and V. Banerjee, *J. Phys. D: Appl. Phys.*, 2013, **46**, 385003.
7. G. Vallejo-Fernandez, O. Whear, A. G. Roca, S. Hussain, J. Timmis, V. Patel and K. O'Grady, *J. Phys. D: Appl. Phys.*, 2013, **46**, 312001.
8. M. Dasha, F. Chiellini, R. M. Ottenbrite and E. Chiellini, *Prog. Polym. Sci.*, 2011, **36**, 981.

9. S. Manzoor, A. Ahmed, A. Rashid, S. N. Ahmad and S. A. Shaheen, *IEEE TRANSACTIONS ON MAGNETICS*, 2013, **49**, 3504.

10. R. Haghniaz, K. R. Bhayani, R. D. Umrani and K. M. Paknikar, *RSC Adv.*, 2013, **3**, 18489.

11. A. Giri, A. Makhal, B. Ghosh, A. K. Raychaudhuri and S. K. Pal, *Nanoscale*, 2010, **2**, 2704.

12. S. Louguet, B. Rousseau, R. Epherre, N. Guidolin, G. Goglio, S. Mornet, E. Duguet, S. Lecommandoux and C. Schatz, *Polymer Chemistry*, 2012, **3**, 1408.

13. N. D. Thorat, R. M. Patil, V. M. Khot, A. B. Salunkhe, A. I. Prasad, K. C. Barick, R. S. Ningthoujam and S. H. Pawar, *New Journal of Chemistry*, 2013, **37**, 2733.

14. R. M. Patil, P. B. Shete, N. D. Thorat, S. V. Otari, K. C. Barick, A. Prasad, R. S. Ningthoujam, B. M. Tiwale and S. H. Pawar, *Journal of Magnetism and Magnetic Materials*, 2014, **355**, 22.

15. J. Qu, G. Liu, Y. Wang and R. Hong, *Advanced Powder Technology*, 2010, **21**, 461.

16. D.-L. Zhao, X.-X. Wang, X.-W. Zeng, Q.-S. Xia and J.-T. Tang, *Journal of Alloys and Compounds*, 2009, **477**, 739.

17. G.-y. Li, Y.-R. Jiang, K.-l. Huang, P. Ding and J. Chen, *Journal of Alloys and Compounds*, 2008, **466**, 451.

18. T. Qiao, Y. Wu, J. Jin, W. Gao, Q. Xie, S. Wang, Y. Zhang and H. Deng, *Colloids and Surfaces A: Physicochemical and Engineering Aspects*, 2011, **380**, 169.

19. K. H. Bae, M. Park, M. J. Do, N. Lee, J. H. Ryu, G. W. Kim, C. Kim, T. G. Park and T. Hyeon, *ACS Nano*, 2012, **6**, 5266.

20. M. M. Song, W. J. Song, H. Bi, J. Wang, W. L. Wu, J. Sun and M. Yu, *Biomaterials*, 2010, **31**, 1509.

21. Y.-H. Lee, F.-Y.Cheng, H.-W.Chiu, J.-C.Tsai, C.-Y.Fang, C.-W.Chen and Y.-J. Wang, *Biomaterials*, 2014, **35**, 4706.

22. J. Blechinger, A. T. Bauer, A. A. Torrano, C. Gorzelanny, C. Brauchle and S. W. Schneider, *Small*, 2013, **9**, 3970-3980, 3906.

23. D. Laha, A. Pramanik, J. Maity, A. Mukherjee, P. Pramanik, A. Laskar and P. Karmakar, *Biochim Biophys Acta*, 2014, **1840**, 1.

24. N. D. Thorat, S. V. Otari, R. M. Patil, V. M. Khot, A. I. Prasad, R. S. Ningthoujam and S. H. Pawar, *Colloids and Surfaces B: Biointerfaces*, 2013, **111**, 264.

25. S. Dutz and R. Hergt, *Int J Hyperthermia*, 2013, **29**,790.

26. N. D. Thorat, S. V. Otari, R. A. Bohara, H. M. Yadav, V. M. Khot, A. B. Salunkhe, M. R. Phadatare, A. I. Prasad, R. S. Ningthoujam and S. H. Pawar, *Materials Science and Engineering: C*, 2014, **42**, 637.

27. S. Rana, N. V. Jadhav, K. C. Barick, B. N. Pandey and P. A. Hassan, *Dalton Trans*, 2014, **43**, 12263.

28. N. D. Thorat, V. M. Khot, A. B. Salunkhe, A. I. Prasad, R. S. Ningthoujam and S. H. Pawar, *J. Phys. D: Appl. Phys.*, 2013, **46**, 105003.

29. N. D. Thorat, V.M. Khot, A. B. Salunkhe, R. S. Ningthoujam and S.H. Pawar *Colloids and Surfaces B: Biointerfaces, 2013,* **104**, 40.

30. D. Yoo, H. Jeong, C. Preihs, J. Choi, T. H. Shin, J. L. Sessler and J. Cheon, *Angew. Chem. Int. Ed.*, 2012, **51**, 12482.

31. S. J. Choi, J. M. Oh and J. H. Choy, *J. Inorg. Biochem.*, 2009, **103**, 463.

Figure Legends:

Fig. 1. Characterization of chitosan functionalized LSMO MNPs. (a) FTIR spectrum showing efficient coating of chitosan on LSMO MNPs chitosan; stretching specific to 1000 cm^{-1} and 1627 cm^{-1} representing C-O primary alcoholic group and N–H bending in chitosan,characteristic peaks of vibration of chitosan. (b) TGA spectra of bare LSMO and LSMO@Chitosan MNPsin nitrogen with a scanning rate of 10°Cmin^{-1}up to 500°C. FESEM (c) and TEM (d) images LSMO@Chitosan MNPs showing the size of MNP and MNPs coated with chitosan.

Fig. 2. Magnetic behavior of MNPs and CH-MNPs measured by VSM, which shows decrease in magnetization after chitosan coating. Measurements are performed at 300 K.

Fig. 3. Colloidal stability by pH dependent zeta potential study of CH-MNPs.

Fig. 4. Biocompatibility of MNPs and CH-MNPs. Cell viability data of MNPs and CH-MNPs for 24 and 48 h on HeLa, L929 and MCF7 cells. Values are expressed as mean ± SD, n = 3.

Fig. 5. Physical interaction of MNPs and cellular phenotype study.DAPI, FITC and PI stained confocal microscopy images of L929 cells incubated with CH-MNPs for 24 h (Panel A to C represents cells treated with 0, 0.2 and 1 mg/mL CH-MNPs, respectively).

Fig. 6 (a) Concentration and field dependent temperature kinetic curves of MNPs and CH-MNPs dispersed in water with a concentration of 2 mg/mL (b) field dependent SAR values of MNPs and CH-MNPs in water. Values are expressed as mean ± SD, n = 3. (c) The percentage viability

of normal and cancer cells treated with MNPs and CH-MNPs. Cells were treated with MNPs and CH-MNPs (1 mg/mL) for 30-120 min followed with or without alternating magnetic field (300 Oe, frequency 267 KHz). After treatment, cells were incubated in culture conditions for 1 h. Cells werethen harvested by trypsinization and followed by a trypan blue viability assay. Values are expressed as mean ± SD, n = 2. (d) Temperature profile for MNPs and CH-MNPs incubated with cancer cells during *in vitro* experiments. (e) Confocal microscopy images of magnetic fluid hyperthermia non treated and treated cancer cells for CH-MNPs after 120 min.

Figure 1

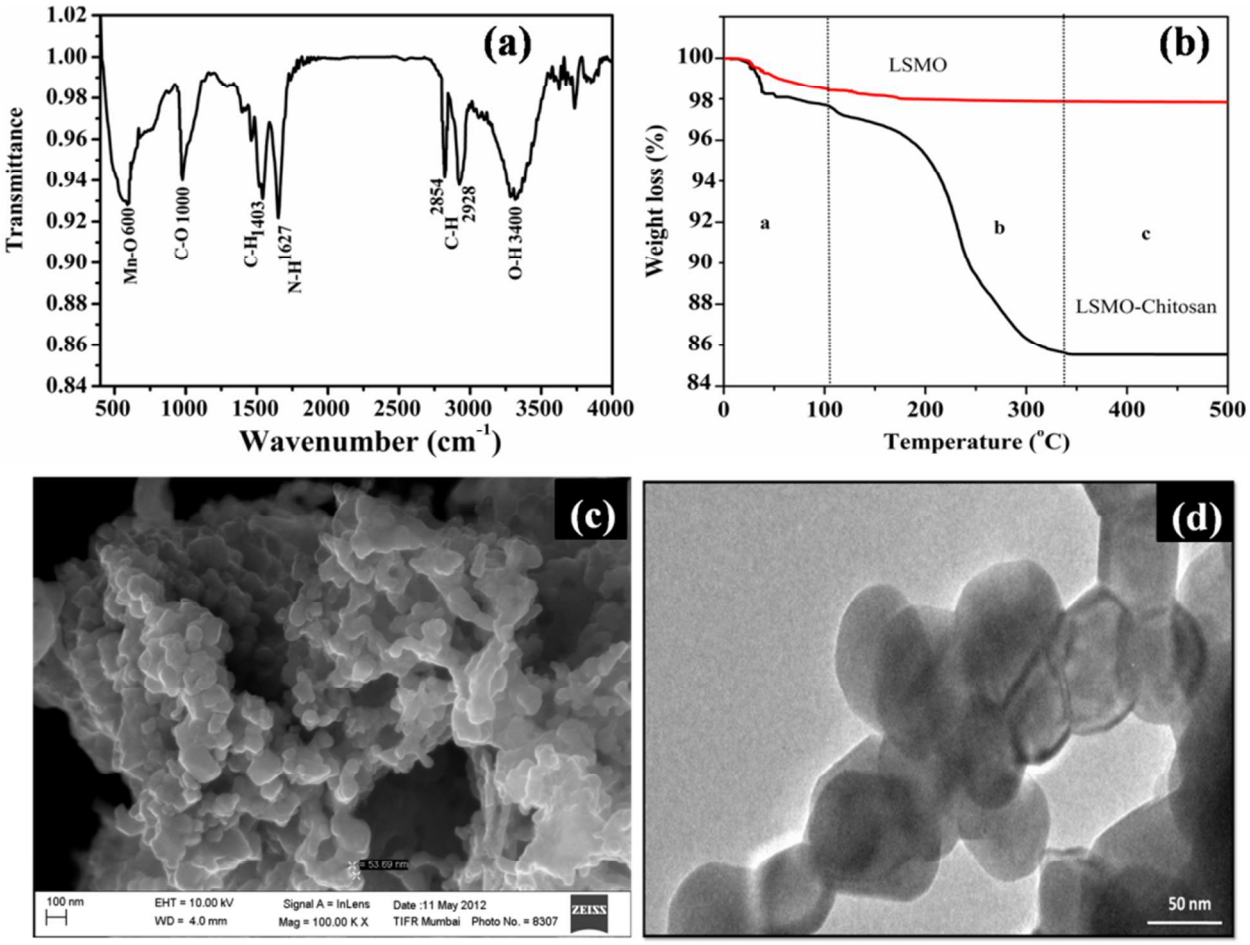

Figure 2

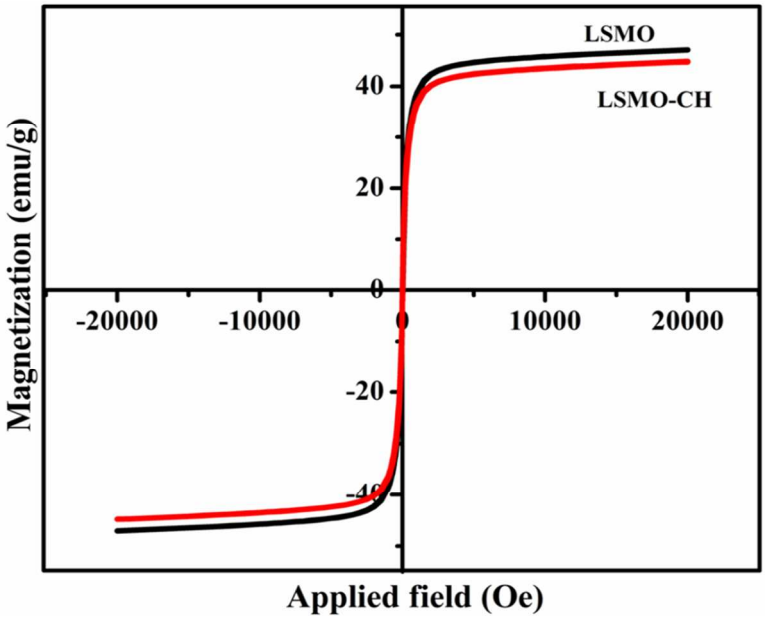

429 **Figure 3**

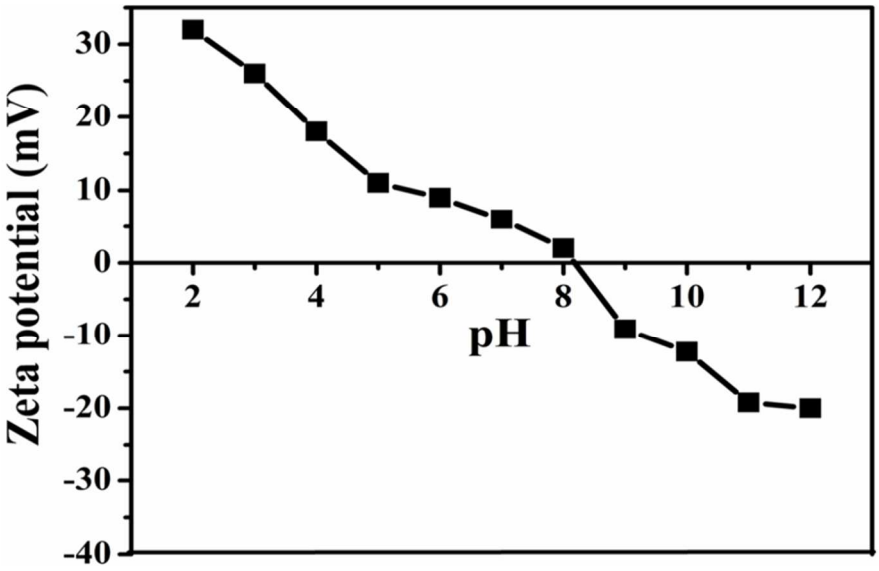

Figure 4

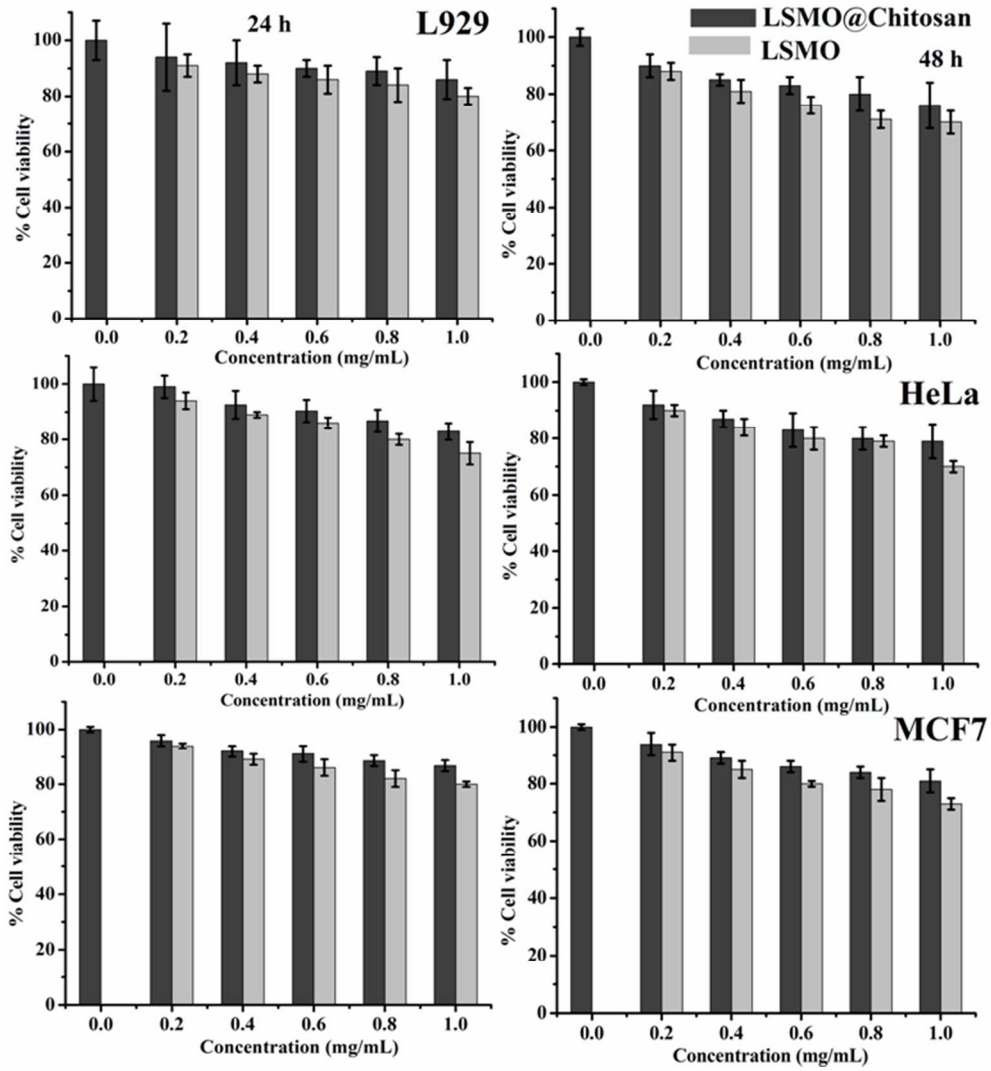

431 **Figure 5**

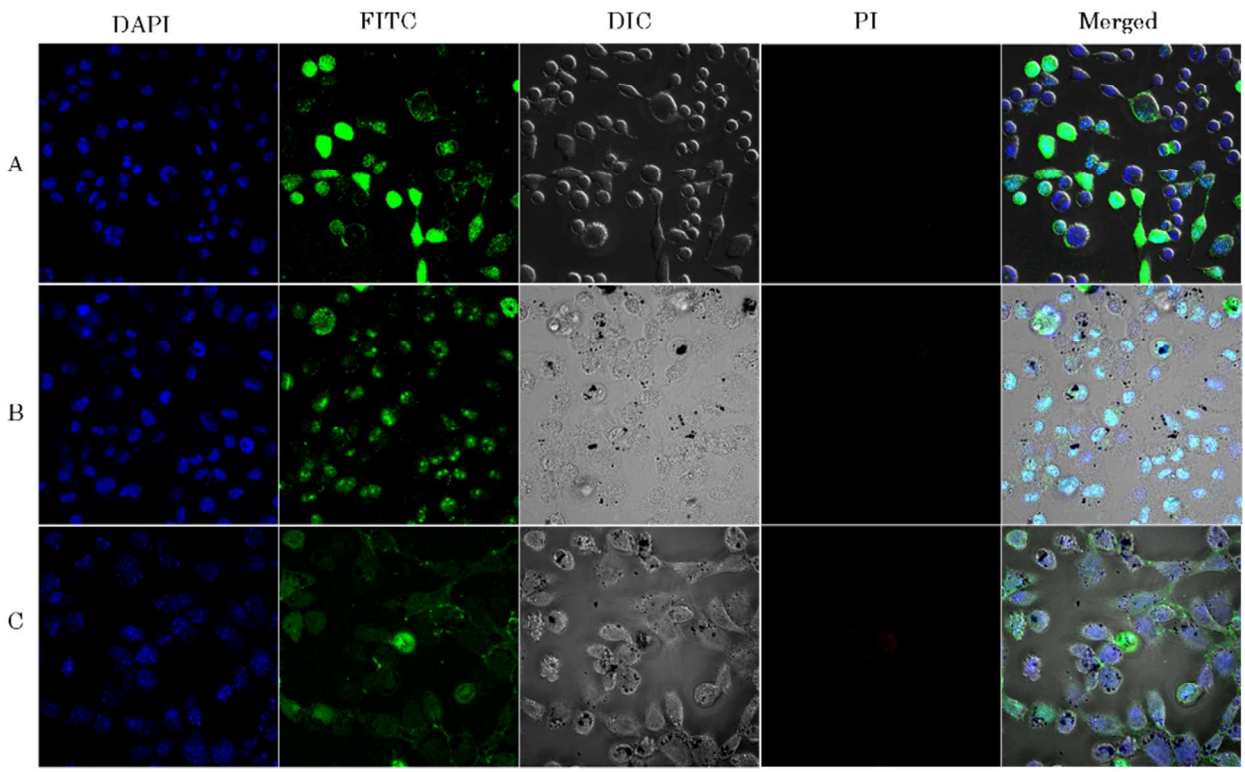

Figure 6

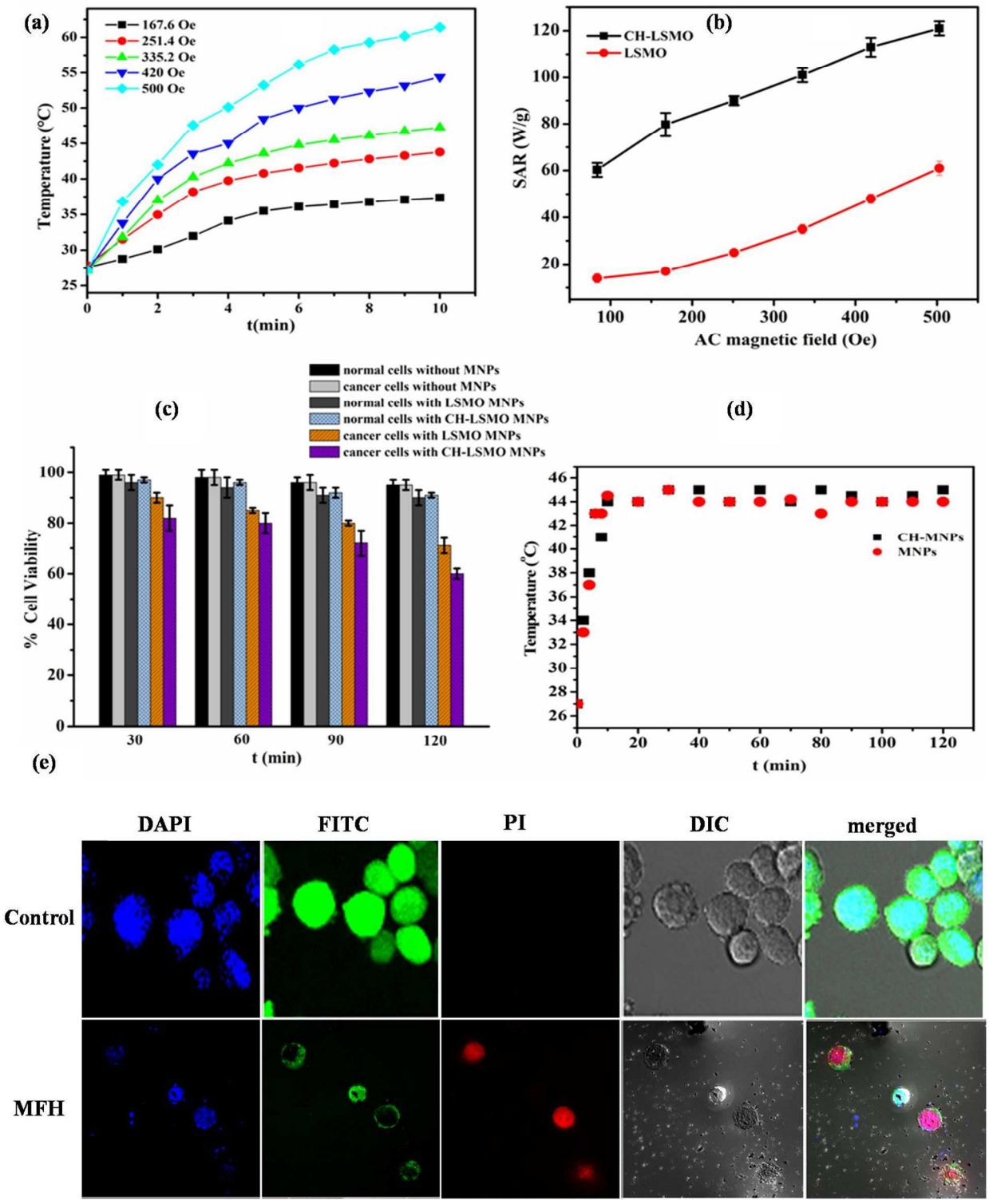

Graphical Abstract

The LSMO-Chitosan core cell formation improves cell viability, colloidal stability and hyperthermia properties and suitable cancer cell acidic environment.